Journal of Computational Physics 227 (2008) 8736–8752

Contents lists available at ScienceDirect

Journal of Computational Physics

journal homepage: www.elsevier.com/locate/jcp

Time-reversibility of the Euler equations as a benchmark for energy conserving schemes

M. Duponcheel [a,*], P. Orlandi [b], G. Winckelmans [a]

[a] Université catholique de Louvain (UCL), Mechanical Engineering Department, Division TERM, Center for Systems Engineering and Applied Mechanics (CESAME), 1348 Louvain-la-Neuve, Belgium
[b] Università di Roma "La Sapienza", Department of Mechanics and Aeronautics, 00184 Roma, Italy

ARTICLE INFO

Article history:
Received 11 May 2007
Received in revised form 25 February 2008
Accepted 20 June 2008
Available online 28 June 2008

Keywords:
Euler equations
Time reversibility
Taylor–Green vortex
Energy conservation
Navier–Stokes solvers
Discretization

ABSTRACT

The three-dimensional incompressible Euler equations are time-reversible. This property should be preserved as well as possible by numerical discretizations. This article investigates the time-reversibility properties of various solvers designed for incompressible Navier–Stokes computations. The test case is the inviscid Taylor–Green vortex, which becomes "turbulent" before the time is reversed to try to recover the initial condition. The simulations are performed using high and low order finite difference solvers as well as using a pseudo-spectral solver. Various time-stepping schemes are also investigated. Although the flow statistics are significantly affected by the accuracy of the space discretization, the time-reversibility is not because most space-discretizations are time-reversible for an exact time-stepping. The crucial factor for time-reversibility is the accuracy of the time-stepping scheme and its interaction with the space-discretization. Furthermore, an important practical requirement for the solver is to be energy conserving in order to avoid numerical instability. An energy conserving solver using an accurate time-stepping is then able to go back almost perfectly from a complex "turbulent" flow to the simple initial condition. Therefore, we propose that this constitutes a severe and useful benchmark that Navier–Stokes solvers should challenge. The present investigations and their conclusions are also supported by parallel 1-D investigations, using the non-linear convection equation (inviscid Burgers) and the linear convection equation.

1. Introduction

It is easily verified that the incompressible continuous Euler equations

$$\nabla \cdot \mathbf{u} = 0, \tag{1a}$$

$$\frac{\partial \mathbf{u}}{\partial t} + (\mathbf{u} \cdot \nabla)\mathbf{u} = -\nabla P, \tag{1b}$$

with $P = p/\rho$ the reduced pressure, are time-reversible. If $(\mathbf{u}(\mathbf{x}, t), p(\mathbf{x}, t))$ is a solution of the system, then $(-\mathbf{u}(\mathbf{x}, -t), p(\mathbf{x}, -t))$ is also a solution. Therefore, if $\mathbf{u}^*(\mathbf{x})$ is the solution at time t^* of the problem with an initial condition $\mathbf{u}_0(\mathbf{x})$ then $-\mathbf{u}_0(\mathbf{x})$ is the solution at time t^* of the problem with an initial condition $-\mathbf{u}^*(\mathbf{x})$. It is legitimate to expect a numerical discretization of the Euler equations to preserve this time-reversibility property. Note also that the time-reversibility property was previously used by Carati et al. [1] to assess models for explicitly filtered LES because the explicit filtering does not alter the time-reversibility of the equations.

* Corresponding author. Tel.: +32 10 474031; fax: +32 10 452692.
E-mail address: matthieu.duponcheel@uclouvain.be (M. Duponcheel).

0021-9991/$ - see front matter © 2008 Elsevier Inc. All rights reserved.
doi:10.1016/j.jcp.2008.06.020

The aim of this paper is to investigate the time-reversibility property of various Navier–Stokes solvers running with the viscosity deliberately set to zero and without any subgrid-scale model. A fully periodic test case was chosen to avoid the possible influence of the boundary conditions. The present study is thus entirely focused on the behavior of the discretization of the convective term and its interaction with the time stepping scheme. This is indeed the more relevant term in high Reynolds number flows.

The initial condition of the present investigation is the simple analytical Taylor–Green vortex. Then, the flow freely evolves and eventually becomes "turbulent". Small-scales are generated and, since there is no viscosity, the energy spectrum $E(k)$ tends to a k^2 behavior at the high wave numbers. Then, the sign of the velocities is changed and the simulation is run further. This is equivalent to going back in time. The ability of the solver to recover the initial condition is then assessed.

Three different energy-conserving space discretizations are compared in the present study: two centered finite difference schemes and a pseudo-spectral method. The first finite difference scheme is second order accurate whereas the second one is fourth order accurate. In all three solvers, two time-stepping schemes are available: a second order Adams–Bashforth scheme (AB2) and a third order Runge–Kutta method (RK3).

It is observed that the accuracy of the spatial discretization does not directly influence the time-reversibility of the solver; even though the flow statistics strongly depend on it. An energy conserving scheme is however absolutely required since, on the one hand, any spurious injection of energy leads to a fast blow up of the computation and, on the other hand, a systematic dissipation of energy obviously makes it impossible to recover the initial condition. Provided the energy is conserved, the time-reversibility mainly depends on the accuracy of the time discretization scheme because it is shown that the solvers would be perfectly reversible if the time-stepping was exact. Hence, for the same spatial discretization, RK3 performs much better than AB2 (which is known to be slightly unstable for purely convective linear problems, even when using a small time step, as done is this investigation). However, the space discretization also interferes with the time-stepping because the accuracy of the time-stepping depends on its eigenvalues. Consequently, in all cases, the present second order finite difference solver is the best at recovering the initial condition among the studied schemes. As the lack of exact energy conservation of the discrete solver is also due to time stepping errors, there is a strong correlation between energy conservation and time-reversibility.

To recover well enough the initial condition, one needs an energy conserving space discretization and an accurate time-stepping. This also ensures that the energy will be very well conserved. Therefore, the present time-reversibility test is proposed as a sensitive test for energy conserving schemes. Those are especially important for Navier–Stokes solvers and also for LES solvers that use explicit subgrid-scale modeling. They are also important to study the non-linear dynamics of the Euler equation (e.g., see [2]) and to try to give answers to fundamental questions such as the possible finite time singularity in the Euler equations. Here, especially, the effects of the numerics must be sufficiently understood before any definite answer can be given.

This paper is organized as follows. Section 2 briefly describes the solvers assessed in this study. Then, Section 3 presents the Taylor–Green vortex test case and the numerical parameters used. The results obtained on this test case are presented in Section 4. They are further analyzed in Section 5 where they are compared to 1D results in order to clearly identify the factors governing the time-reversibility properties.

2. Numerical methods

This section describes first the two finite difference solvers (referred to as FD2 and FD4) and then the pseudo-spectral solver (PS) used in this investigation.

2.1. Finite difference solvers

Both finite difference codes solve the incompressible Navier–Stokes equations on Cartesian MAC grids. The equations are integrated in time using a fractional-step method introducing the pressure gradient in the computation of the intermediate velocity. It was called the "delta" form for the pressure by Lee et al. [3]. This form allows simple boundary conditions for the pressure and the intermediate velocity field. When the convective term is integrated using AB2, the time-stepping scheme reads

$$\frac{\mathbf{u}^* - \mathbf{u}^n}{\Delta t} = -\frac{1}{2}\left(3\mathbf{H}^n - \mathbf{H}^{n-1}\right) - \nabla P^n, \tag{2a}$$

$$\nabla^2 \varphi = \frac{1}{\Delta t}\nabla \cdot \mathbf{u}^*, \tag{2b}$$

$$\frac{\mathbf{u}^{n+1} - \mathbf{u}^*}{\Delta t} = -\nabla \varphi, \tag{2c}$$

$$P^{n+1} = P^n + \varphi, \tag{2d}$$

where $\mathbf{H}^n$ is the convective term, $\mathbf{u}^*$ is the intermediate velocity field and P^n is the reduced pressure. Two time-stepping schemes are available in both solvers: AB2 and RK3. In RK3, the divergence-free constraint in enforced at each substep.

2.1.1. Second order solver (FD2)

The convective term is discretized in the divergence form $(\partial(u_i u_j)/\partial x_j)$ using second order centered differences and interpolations. This discretization of the convective term conserves a priori the momentum and it conserves the energy provided that the solution is numerically divergence-free (see [4]). The Poisson equation for the pressure is solved using a direct method. The problem is decomposed in Fourier modes in the x- an y-directions while it is discretized using second order finite differences in the z-direction. Modified wave numbers are introduced to ensure the discrete mass conservation. This finally leads to tridiagonal systems to solve. The whole solver is described in detail in [5].

2.1.2. Fourth order solver (FD4)

The equations are discretized in space using the fourth order finite difference scheme of Vasilyev [6]. The skew-symmetric form of the discretization of the convective term, that is used here, is designed to a priori conserve energy on Cartesian stretched meshes. The Poisson equation for the pressure is solved using an efficient iterative multigrid solver, with a Gauss–Seidel smoother, up to a prescribed low level residual.

2.2. Pseudo-spectral solver (PS)

This code is based on the pseudo-spectral methodology. The incompressible Euler equations are solved in the Fourier space. If one used an explicit Euler time-step, this would read

$$\frac{\widehat{u}_i^{\,*} - \widehat{u}_i^{\,n}}{\Delta t} = -Ik_j \widehat{u_i^n u_j^n}, \tag{3a}$$

$$\widehat{u}_i^{\,n+1} = \widehat{u}_i^{\,*} - k_i \frac{k_j \widehat{u}_j^{\,*}}{k_m k_m} \tag{3b}$$

with $I^2 = -1$, and where $\widehat{(\cdot)}$ corresponds to the Fourier transform and $\mathbf{k}$ is the wave number. The equations are here integrated in time using the RK3 scheme of Williamson [7] or the AB2 scheme. The incompressibility constraint is imposed at each substep of the RK3 scheme. The non-linear term is evaluated pseudo-spectrally using fast Fourier transforms. In order to conserve the energy, the code is fully dealiased by applying the 2/3 rule (see [8]). By default, a spherical truncation in the Fourier space is also applied: the modes with $|\mathbf{k}| > n/2$ are set to zero. For the cases where the spherical truncation is not used, the solver will be referred to as $\mathrm{PS}_{\mathrm{w/oT}}$.

3. Numerical setup

The simulation is initialized using the Taylor–Green vortex:

$$u = \sin(x)\cos(y)\cos(z), \tag{4a}$$

$$v = -\cos(x)\sin(y)\cos(z), \tag{4b}$$

$$w = 0. \tag{4c}$$

This can be decomposed as the sum of eight Fourier modes of equal wavelength $|\mathbf{k}| = \sqrt{3}$ so that its discrete spectrum only has one non-zero mode ($E(k = 2)$). The domain is the periodic cubic box of periodicity $L = 2\pi$, here discretized using 96 grid points in each direction. The time step used in all simulations is very small: $\Delta t = 10^{-3}$.

The simulation is run until a time t_{rev} (forward simulation), after which the time is reversed. This time reversal is simply obtained by switching the sign of the velocity field. The simulation is then run again for the same number of time steps as before (backward simulation), so that an ideal solver should recover exactly the initial condition. As the Adams–Bashforth scheme is not self-starting, the time reversal is somewhat trickier: one computes an additional time-step in the forward simulation, and it can be used to compute the first time-step of the backward simulation.

4. Results

The Taylor–Green Vortex evolves naturally from its very simple initial condition because of its initial pressure gradient in z. It eventually undergoes a transition to high complexity and "turbulence". The initial phase of the flow was studied in detail by Brachet et al. [9] using direct numerical simulation (DNS) at various Reynolds numbers. As the problem is here solved without explicit dissipation, the energy piles up in the highest wave numbers of the spectrum leading to $E(k) \propto k^2$. The resulting "turbulent" flow has no physical meaning but is here used to investigate the time-reversibility of the solvers: they should be able to go back from this complex field to the simple initial condition.

Hereafter, the behavior of the three solvers is compared in two cases: first, AB2 is used and the time reversal occurs at $t_{\mathrm{rev}} = 8$, second, RK3 is used and the time reversal occurs at $t_{\mathrm{rev}} = 10$. Then, the influence of the resolution is studied for both time-stepping schemes with $t_{\mathrm{rev}} = 8$ and, finally, the influence of the time reversal time is studied for the combination FD4-AB2.

4.1. Comparison of the solvers using AB2

For the first comparison of the solvers, the time reversal occurs at $t_{\text{rev}} = 8$ when the flow is already very complex.

The flow field at times of interest is visualized in Fig. 1 using iso-surfaces of the λ_2 criterion as defined in Jeong and Hussain [10] obtained using FD4 and AB2. This clearly reveals the high complexity of the flow when the time is reversed, after 8000 time-steps. We can also compare the initial condition and the flow field obtained after the backward simulation.

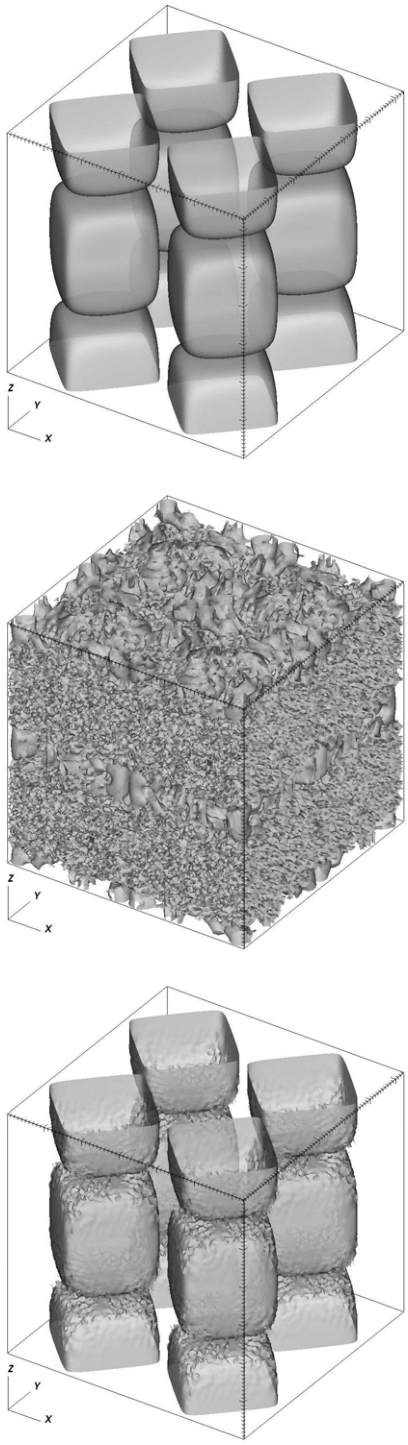

Fig. 1. Visualization of the flow using one iso-surface of $\lambda_2 = -0.025$ for the case FD4-AB2 with time reversal at $t_{\text{rev}} = 8$: $t = 0$ (above), $t_{\text{rev}} = 8$ (center) and $t = 16$ (below).

The large-scale structures of the two fields are very similar, yet some wiggles are visible after the backward simulation. This denotes that some high wave number modes have been energized compared to the initial condition. However, this already shows the very good time-reversibility properties of the solver, that will be further detailed later using quantitative diagnostics.

Since there is no dissipation term, the energy $E = \frac{1}{2}\langle u_i u_i \rangle$ should be conserved. Fig. 2 shows that, even for the worst case, the maximum error on the energy conservation is very small (about 0.01% of the initial energy). The global behavior of all the numerical schemes is globally anti-diffusive as should be expected since the AB2 scheme is slightly unstable for convection problems. The energy starts to increase significantly when the flow becomes highly three-dimensional. However, a significant part of the energy conservation error appears to be reversible since the energy in seen to decrease after the time reversal. At the end of the backward simulation, it finally stabilizes at a slightly higher level than the initial energy. All codes perform very similarly, although the present FD2 scheme slightly outperforms the other schemes: it reaches a lower plateau at the end of the backward simulation.

The time history of the turbulence intensities is shown in Fig. 3. Because of the initial symmetry, the evolutions of $\langle u^2 \rangle$ and $\langle v^2 \rangle$ are identical; hence only $\langle u^2 \rangle$ is shown in Fig. 3. Starting from a quasi two-dimensional configuration, the flow evolves by energizing the w-component. When the "turbulence" is well established, the mean square components reach an almost constant, but different, value. This denotes that a significant anisotropy of the flow is still present. After $t \simeq 6$, the results depend significantly on the solvers. The differences are related to the differences in truncation errors (i.e. order) and also in dispersion errors. As far as the time-reversibility is concerned, the evolutions are almost perfectly symmetrical with respect to time reversal at $t_{\text{rev}} = 8$. However, the zoom at the end of the evolution for $\langle w^2 \rangle$ in the backward simulation (Fig. 3) shows that the present FD2 solver recovers the initial condition slightly better than the present FD4, PS and $\text{PS}_{\text{w/oT}}$ solvers do: $\langle w^2 \rangle_{\text{FD2}} < \langle w^2 \rangle_{\text{FD4}} < \langle w^2 \rangle_{\text{PS}} < \langle w^2 \rangle_{\text{PSwoT}}$.

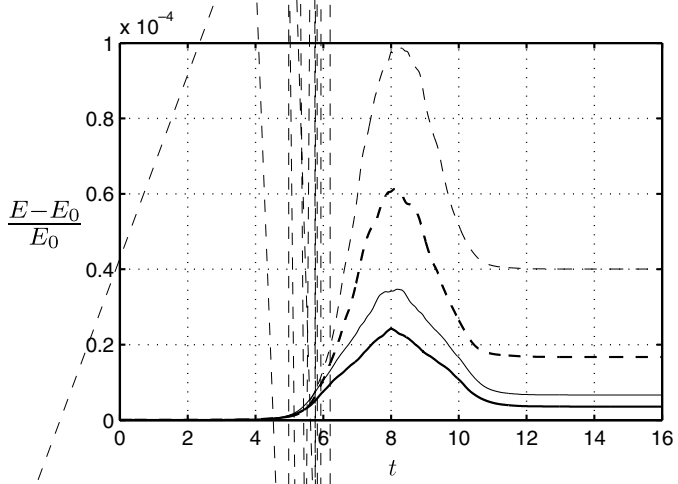

Fig. 2. Time history of $(E - E_0)/E_0$ obtained using FD2 (thick solid), FD4 (thin solid), PS (thick dash) and $\text{PS}_{\text{w/oT}}$ (thin dash), all using AB2 and $t_{\text{rev}} = 8$.

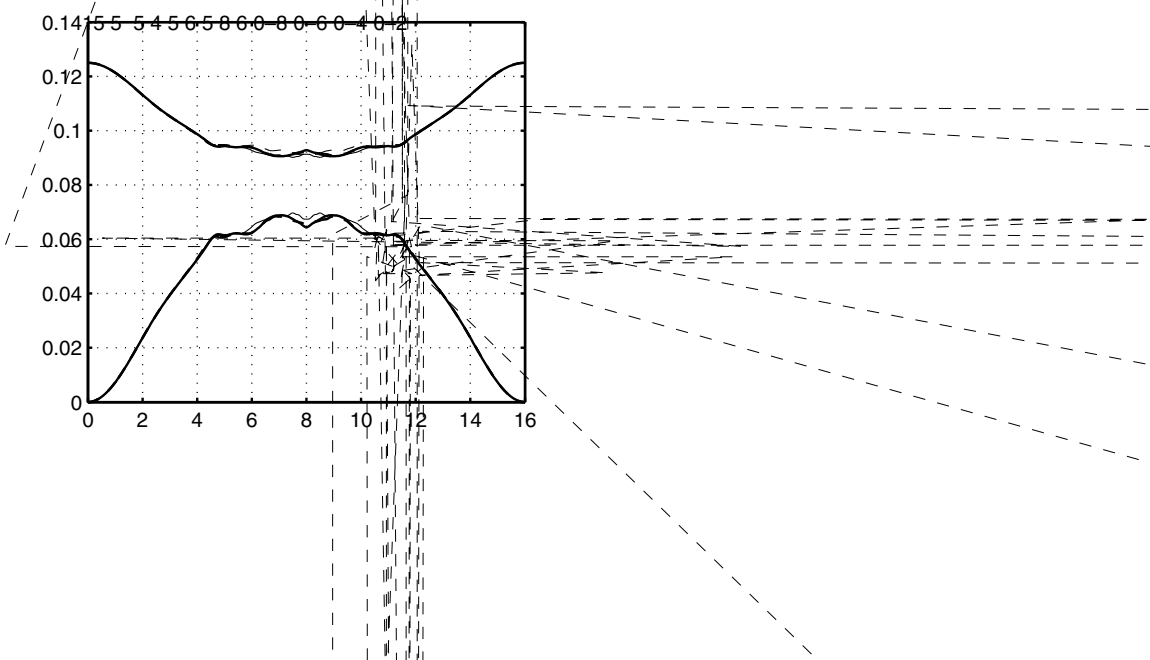

The enstrophy $\mathscr{E} = \frac{1}{2}\langle \omega_i \omega_i \rangle$ is a diagnostic that is much more sensitive to the small-scale structures than the energy. Its time history is shown in Fig. 4. The enstrophy increases monotonically in the forward simulation, as energy is transferred from the large initial scales of the flow to the smaller generated scales. In the backward simulation, the solvers are able to withdraw energy from the small scales to transfer it back to the large ones. The global trend of both solutions is identical, but the maximum enstrophy obtained using FD2 is 30% lower that the maximum value obtained using FD4, as expected because of the higher order. However, the PS solver reaches a lower maximum enstrophy than FD4 does because the spherical truncation removes high wave number modes that contribute significantly to the enstrophy. Indeed, the enstrophy obtained with $\mathrm{PS}_{\mathrm{w/oT}}$ is well above that obtained using FD4. Globally, all solvers succeed very well in going back in time and the error after the backward simulation is small. Yet, the best recovery of the initial value is obtained using FD2, as already observed. Furthermore, the maximum entrophy does not determine the time-reversibility performance of the solvers since the FD4 solver better recovers the initial enstrophy than the PS solver does.

The energy spectra are shown in Fig. 5, in order to better understand the energy transfer achieved between the various scales of the problem. The initial spectrum only has one wave number for which the energy is non-zero. At the end of the forward simulation, the energy is equally distributed among the last modes of the spectrum (equipartition of energy). The spectrum is then proportional to the area of the wave number shell: $E(k) \propto k^2$. Consequently, the compensated energy spectra $k^{-2}E(k)$ should exhibit a plateau; Fig. 5 indeed exhibits such a plateau at $t = t_{\mathrm{rev}}$ for all solvers. For the high wave numbers, the spectrum obtained using PS is slightly above that obtained using the others. This is mainly because the other solvers have energized modes that are beyond the last spherical shell of the spectrum. During the backward simulation, the three solvers succeed in backscattering energy from the high wave numbers to the low wave numbers. At the end, the amplitude of the only one mode of the Taylor–Green vortex is well recovered, while the remaining "noise" of the spectra is almost fully equipartitioned but at a very low level. This is especially true for FD4, PS and $\mathrm{PS}_{\mathrm{w/oT}}$. This "noise" corresponds to the wiggles that can be observed in Fig. 1 at time $t = 16$. For FD2, there is equipartition except for $k = 3, 4, 5$. In particular, the mode $k = 3$ is

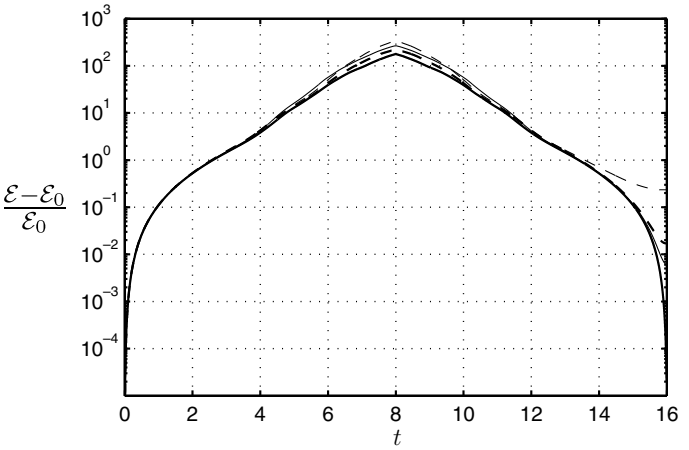

Fig. 4. Time history of the enstrophy $(\mathscr{E} - \mathscr{E}_0)/\mathscr{E}_0$ obtained using FD2 (thick solid), FD4 (thin solid), PS (thick dash) and $\mathrm{PS}_{\mathrm{w/oT}}$ (thin dash), all using AB2 and $t_{\mathrm{rev}} = 8$.

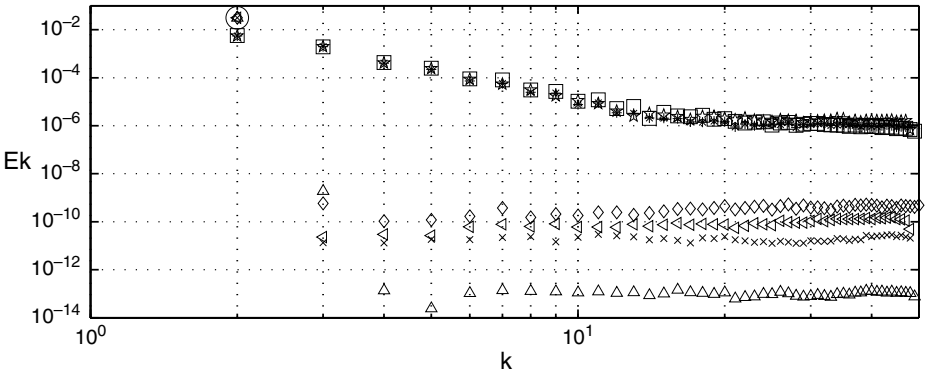

Fig. 5. Compensated energy spectra $k^{-2}E(k)$ at times $t = 0$ (○), $t = 8$ (FD2 (□), FD4 (∗), PS (★) and $\mathrm{PS}_{\mathrm{w/oT}}$ (·)) and $t = 16$ (FD2 (△), FD4 (×), PS (◁) and $\mathrm{PS}_{\mathrm{w/oT}}$ (◇)), all using AB2 and $t_{\mathrm{rev}} = 8$.

quite energized. The spurious energy content of the high wave number modes is less in the present FD2 solver than in the present FD4 and PS solvers; they are however very low for all solvers.

When the forward simulation is run further in time than $t = 8$, the accumulation of errors prevents the solvers from recovering the initial condition after the backward simulation. For instance, Fig. 6 shows the results obtained using FD4 with AB2 and time reversal at $t_{rev} = 10$. The relative error of energy conservation continues to grow after the time reversal and the plateau that is reached at the end of the backward simulation is much higher than in the previous case with $t_{rev} = 8$ (Fig. 2). Also, the time history of $\langle u^2 \rangle$ is no longer symmetrical with respect to $t_{rev} = 10$. The statistics of the flow field after the backward simulation are significantly different from the initial condition. A similar behavior is also obtained when using $t_{rev} = 8$ (as in the reference case) but with larger timesteps.

4.2. Comparison of the solvers using RK3

For the same spatial discretization, Fig. 6 shows that the RK3 time-stepping scheme outperforms the AB2 scheme because it is stable for convection problems but mainly because it is more accurate. The time-reversibility of the combination FD4-RK3 is much better than FD4-AB2. Therefore, the comparison between the solvers using RK3 is performed using the challenging case $t_{rev} = 10$.

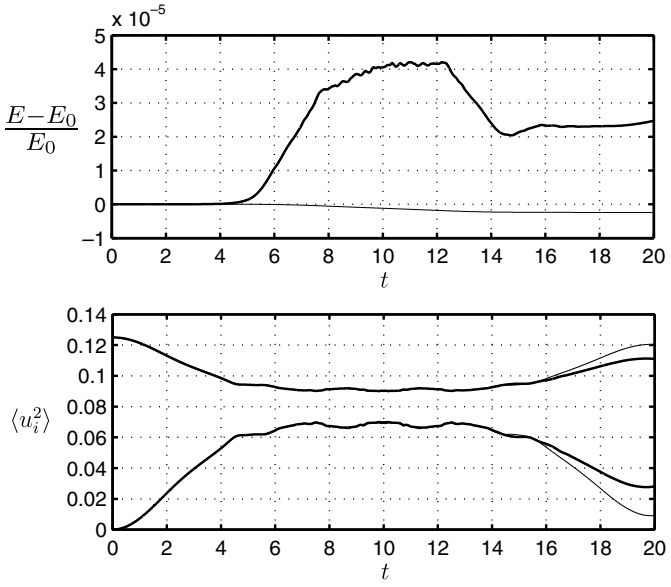

Fig. 6. Time history of $(E - E_0)/E_0$ (above) and time history of $\langle u^2 \rangle = \langle v^2 \rangle$ and of $\langle w^2 \rangle$ (below) obtained using FD4 and AB2 (thick) or RK3 (thin) and time reversal at $t_{rev} = 10$.

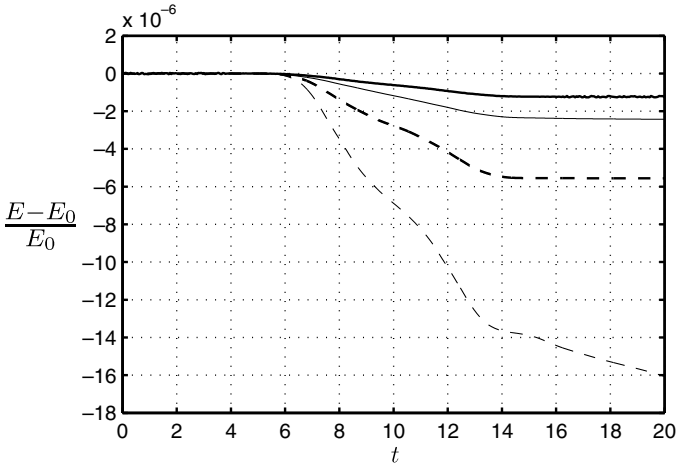

Fig. 7. Time history of $(E - E_0)/E_0$ obtained using FD2 (thick solid), FD4 (thin solid), PS (thick dash) and $PS_{w/oT}$ (thin dash), all using RK3 and $t_{rev} = 10$.

The time history of the energy shown in Fig. 7 is totally different from that shown in Fig. 2. The energy obtained using RK3 is decreasing. This is a consequence of the stability of the RK3 scheme for convection problems. However, the energy continues to decrease monotonically after the time reversal, whereas AB2 had a different behavior in the forward and in the backward simulations. Finally, the smallest loss of energy is obtained using FD2. The loss of energy increases with the order of the scheme. It can also be observed that the loss of energy increases significantly when the spherical truncation is removed in the PS solver. Furthermore, the energy is still decreasing after $t = 14$ whereas it reaches a plateau for the other solvers.

The time history of the turbulence intensities is shown in Fig. 8. The four evolutions are very close to each other until $t = 8$. Then, $\langle w^2 \rangle$ obtained using $\mathrm{PS}_{\mathrm{w/oT}}$ is more energized than the others; $\langle w^2 \rangle_{\mathrm{FD2}}$ being the least energized. Again, this is due to truncation and dispersion errors. The backward simulation leads to two different behaviors. First, FD2 and PS give nearly symmetrical evolutions, i.e. very good time-reversibility, and only the zoom of the end of the time-history of $\langle w^2 \rangle$ reveals a small error. Second, the evolutions obtained using FD4 and $\mathrm{PS}_{\mathrm{w/oT}}$ are asymmetrical but close to each other. Eventually, they end up with a significantly energized $\langle w^2 \rangle$. This two different behaviors are also very clear in the time history of the enstrophy in Fig. 9. The time histories obtained using FD2 and PS are very symmetrical yet, at the end of the backward simulation, the enstrophy obtained using PS is slightly larger than that of the initial field. The enstrophy evolutions obtained using FD4 and $\mathrm{PS}_{\mathrm{w/oT}}$ are asymmetrical since they increase again after $t \simeq 15$. The final enstrophy obtained using $\mathrm{PS}_{\mathrm{w/oT}}$ is larger than that obtained using FD4. It can also be observed that the maximum enstrophy obtained using PS is again smaller than that obtained using FD4. But, when the spherical truncation is removed, the maximum enstrophy is larger than that obtained using FD4, as expected.

The compensated energy spectra $k^{-2}E(k)$ are shown in Fig. 10. They are very similar to those previously obtained in Fig. 5. The plateau in the highest wave numbers is visible just before the time reversal. All spectra are very close to each other. That

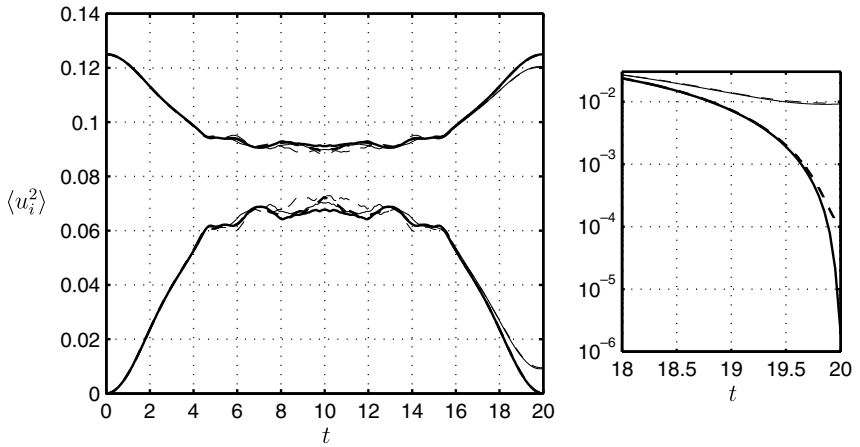

Fig. 8. Time history of $\langle u^2 \rangle = \langle v^2 \rangle$ (curves above) and of $\langle w^2 \rangle$ (curves below) obtained using FD2 (thick solid), FD4 (thin solid), PS (thick dash) and $\mathrm{PS}_{\mathrm{w/oT}}$ (thin dash), all using RK3 and $t_{\mathrm{rev}} = 10$. Zoom at the end of the $\langle w^2 \rangle$ evolution (right).

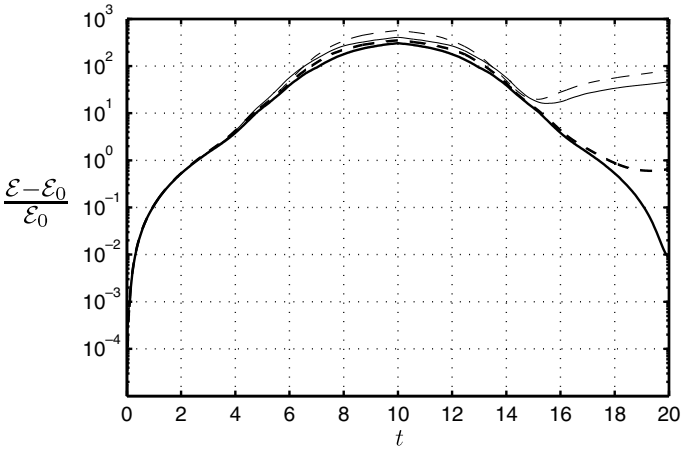

Fig. 9. Time history of the enstrophy $(\mathscr{E} - \mathscr{E}_0)/\mathscr{E}_0$ obtained using FD2 (thick solid), FD4 (thin solid), PS (thick dash) and $\mathrm{PS}_{\mathrm{w/oT}}$ (thin dash), all using RK3 and $t_{\mathrm{rev}} = 10$.

obtained using the PS solver is slightly above the others because the spherical truncation restrains the energy transfer to fewer modes that are thus more energized. Compared to the results obtained using AB2, the level of the "noise" after the backward simulation is significantly larger for the solvers. This confirms that this case is much more challenging than the previous one. Finally, the energy spectra at $t = 20$ demonstrate that the present FD2 solver has better time-reversibility capabilities than the other solvers. It is also seen than the FD2 and PS solvers are such that the energy of the noise is equi-

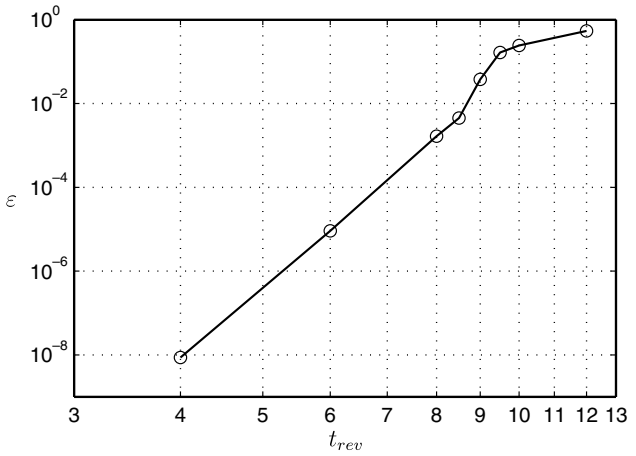

Fig. 12. Evolution of the L2-norm of the error ε on the field obtained after the backward simulation as a function of the time reversal time t_{rev} obtained using FD4-AB2 for a fixed grid and time-step.

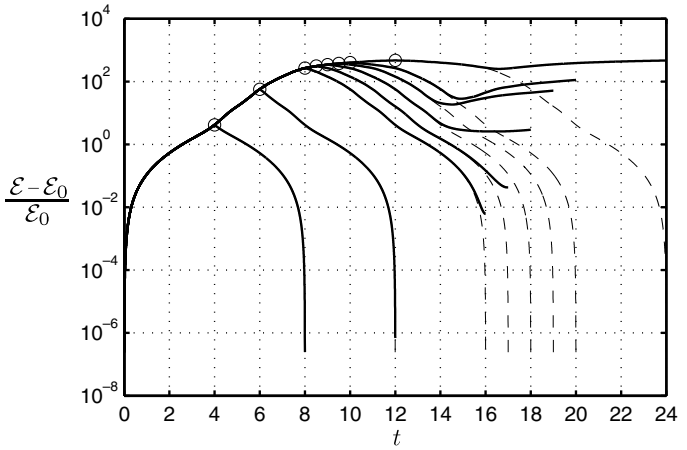

Fig. 13. Time history of the enstrophy $(\mathscr{E} - \mathscr{E}_0)/\mathscr{E}_0$ obtained using FD4-AB2 (solid) for various reversal times t_{rev} with fixed grid and time-step. The time reversal for each case is marked with a circle. The curves in dash are the ideal backward simulations for each case

4.4. Influence of the time reversal time

The influence of the time-reversal time is studied in more detail for the combination FD4-AB2. The resolution and the time-step are taken as in Section 3 and are kept constant. The time reversibility test is performed using several values for t_{rev} lying in the interval $[4; 12]$.

Fig. 12 shows the L2-norm of the error after the backward simulation with respect to the initial condition for the various time reversal times. The error always increases when t_{rev} increases. However, for $t_{\text{rev}} > 8.5$, the error first increases faster then tends to saturate. Fig. 13 shows the time history of the enstrophy of all simulations reported in Fig. 12. The fast increase of the error corresponds to cases where the enstrophy increases at the end of the backward simulation, although it should decrease monotonically during the whole backward simulation. This behavior was already observed in Fig. 9.

5. Further analysis and discussion

The results above show that the present FD2 solver is better at recovering the initial condition than the present FD4 and PS solvers. It may seem surprising that a low order numerical method outperforms higher order methods and that coarsening the grid improves the time-reversibility. This section is devoted to the explanation of this behavior. It will be shown that the accuracy of the time-stepping is critical while the spatial accuracy does not directly influence the time-reversibility. Also, energy conservation is shown to be required to be able to perform both the forward and the backward simulation.

If one assumes an exact time-stepping, the semi-discrete Euler equations read

$$\nabla^h \cdot \mathbf{u}^h = 0, \tag{5a}$$

$$\frac{\mathrm{d}\mathbf{u}^h}{\mathrm{d}t} + \mathbf{H}^h(\mathbf{u}^h) = -\nabla^h P^h, \tag{5b}$$

where $\mathbf{H}^h(\mathbf{u}^h)$ is the discretized convective term. Similarly to the continuous case, this system is time reversible if

$$\mathbf{H}^h(\mathbf{u}^h) = \mathbf{H}^h(-\mathbf{u}^h). \tag{6}$$

This condition is not very restrictive because it is verified by most basic discretizations of the convective term. Notable exceptions are upwind biased schemes that are of course not reversible.

The symmetry condition (6) shows that the time-reversibility is intrinsically independent of the accuracy, i.e. the order, of the space discretization. It is a matter of symmetry rather than a matter of precision. Moreover, it also implies that most of the errors introduced by a space discretization scheme satisfying (6) are reversible and do not affect its time reversibility. Examples of classical errors introduced by a discrete convective term are dispersion errors or aliasing errors: they are both reversible. This is illustrated later in this section by using basic 1D problems.

Although the condition (6) does not imply energy conservation, it obviously implies a symmetry in its evolution. Indeed, the evolution of the energy of the semi-discrete solution is governed by

$$\frac{1}{2}\frac{\mathrm{d}}{\mathrm{d}t}((\mathbf{u}^h, \mathbf{u}^h)_h) + (\mathbf{u}^h, \mathbf{H}^h(\mathbf{u}^h))_h = 0, \tag{7}$$

where $(\cdot,\cdot)_h$ is defined as

$$(\mathbf{u}^h, \mathbf{v}^h)_h = \frac{1}{V}\sum_{i=1}^{N} \mathbf{u}^h(\mathbf{x_i}) \cdot \mathbf{v}^h(\mathbf{x_i}) \Delta V_i, \tag{8}$$

where V is the total volume of the domain and ΔV_i is the volume associated to each unknown (here identical). When the sign of the velocity is changed, Eq. (7) becomes

$$\frac{1}{2}\frac{\mathrm{d}}{\mathrm{d}t}((-\mathbf{u}^h, -\mathbf{u}^h)_h) + (-\mathbf{u}^h, \mathbf{H}^h(-\mathbf{u}^h))_h = 0. \tag{9}$$

If the scheme satisfies (6), then

$$\frac{\mathrm{d}}{\mathrm{d}t}((-\mathbf{u}^h, -\mathbf{u}^h)_h) = -\frac{\mathrm{d}}{\mathrm{d}t}((\mathbf{u}^h, \mathbf{u}^h)_h). \tag{10}$$

This relation means that a reversible non-energy conserving schemes that tends to inject or remove energy from the flow in the forward simulation tends to remove or inject energy, respectively, in the backward simulation. Thus, there is always, at a certain time (either in the forward or in the backward simulation), an injection of energy that usually leads to a blow up of the computation. An example of such behavior can be obtained using the PS solver without any dealiasing procedure: the energy is no longer conserved and the forward simulation blows up. Therefore, energy conservation is a practical requirement to pass the time-reversibility test. Furthermore, among all schemes that are stable, i.e.

$$\frac{\mathrm{d}}{\mathrm{d}t}((\mathbf{u}^h, \mathbf{u}^h)_h) \leqslant 0 \tag{11}$$

for any field $\mathbf{u}^h$, only energy conserving schemes can be time-reversible since the others cannot satisfy Eq. (10).

Consequently, the key of the time-reversibility lies in the time-stepping scheme. Indeed, the condition (6) is sufficient to prove the time reversibility of the semi-discrete system (5) because the exact time derivative is invariant to the simultaneous change of the sign of the velocity and the reversal of the time-line. For a discrete time integration, if the same invariance holded, it would mean that for any time series $\{\mathbf{u}^0, \mathbf{u}^1, \mathbf{u}^2, \ldots, \mathbf{u}^{n-1}, \mathbf{u}^n\}$ being solution of the problem, the time series $\{-\mathbf{u}^n, -\mathbf{u}^{n-1}, \ldots, -\mathbf{u}^2, -\mathbf{u}^1, -\mathbf{u}^0\}$ would also be a solution. So that the fully discrete scheme would be time-reversible. Unfortunately, this does not hold for most time-stepping schemes. For instance, the explicit Euler scheme

$$\mathbf{u}^{n+1} - \mathbf{u}^n = \Delta t \mathbf{F}(\mathbf{u}^n) \tag{12}$$

is clearly not invariant to the simultaneous change of the sign of the velocity and the reversal of the time-line because it then reads

$$-\mathbf{u}^n - (-\mathbf{u}^{n+1}) = \Delta t \mathbf{F}(-\mathbf{u}^{n+1}) = \Delta t \mathbf{F}(\mathbf{u}^{n+1}) \tag{13}$$

that is not equivalent to Eq. (12) since $\mathbf{F}(\mathbf{u}^n) \neq \mathbf{F}(\mathbf{u}^{n+1})$. A family of schemes that are invariant and therefore time-reversible are the time-centered schemes, e.g. Leapfrog, Crank–Nicolson or Pierce's scheme [11]. The time-stepping schemes that are used in the present study, i.e. AB2 and RK3, do not satisfy the invariance property: they are not exactly time-reversible. Therefore, the backward simulation does not coincide exactly with the forward simulation. This "symmetry error" is

basically an accumulation of time-stepping errors and so its amplitude naturally depends on the accuracy of the scheme. This explains that RK3 outperforms AB2.

Although the space discretizations used in this study satisfy the condition (6), it was observed that the time-reversibility of the fully discrete solver also depends on the space discretization when the same time-stepping is used. Since only irreversible time-stepping schemes were used, this denotes a dependence of the time integration errors on the space discretization. Indeed, basic numerical analysis shows that the time-stepping error on each mode of the solution of a linear problem is an increasing function of $\lambda\Delta t$ where λ is the eigenvalue associated to this mode. For instance, in the case of the 1-D linear convection equation

$$\frac{\partial u}{\partial t} + c\frac{\partial u}{\partial x} = 0, \tag{14}$$

the eigenvalue of the mode of wave number k is

$$\lambda = -\mathrm{i}ck. \tag{15}$$

When the equation is discretized in space, its eigenvalues become

$$\lambda = -\mathrm{i}ck_{\mathrm{mod}}(k). \tag{16}$$

where $k_{\mathrm{mod}}(k)$ is the modified wave number of the spatial discretization. The key concept here is that λ has a similar role as Δt. So, obviously, different space discretizations with different eigenvalues have different time-stepping errors. Usually, $k_{\mathrm{mod}}(k)$ (and thus λ) increases when the order of the space discretization increases and therefore, for a fixed time step, the time-stepping error also increases. Recall that this increasing error, the one relevant for the time-reversibility, is the error with respect to the exact time integration of the semi-discrete equations and not to the continuous solution. The latter can be large for low order schemes because of the error induced by the space discretization with respect to the continuous problem. Furthermore, another way to modifying the eigenvalues of the problem is to modify k_{max}, i.e. to change the resolution. Indeed, coarsening the grid reduces the number of modes present in the solution by removing the highest wave number modes. This also reduces the largest eigenvalue. So, if the time-step is kept constant, the time-stepping error decreases. And the time-reversibility increases.

The accuracy of the time-stepping also determines the conservation properties of the fully discrete solvers since the space discretizations used here conserve energy assuming an exact time integration. As already mentioned, λ and Δt play similar roles in the accuracy of the time-stepping and thus, using a higher order space discretization reduces the accuracy and deteriorates the energy conservation. As they both depend on the accuracy of the time-stepping, energy conservation and time-reversibility are clearly correlated.

Even if the above argument has been developed for linear problems, its conclusions are consistent with the results obtained in the 3D benchmark when $t_{\mathrm{rev}} = 8$. The inverse dependence of the time-stepping error on the order of the space discretization explains that the present FD2 solver is better at recovering the initial solution than the other solvers and that the present FD4 solver is better than the present PS solver. Furthermore, the time-reversibility of the PS solver is improved when the spectral truncation is added because it removes the highest wave number modes. They are associated to large eigenvalues, i.e. stiff time-evolution problems, and thus with large time-stepping errors. Again, the improvement of the time-reversibility by the coarsening of the grid can also be explained by the reduction of the maximum eigenvalue due to the coarsening. In other words, the coarsening removes the stiffest modes of the solution and the problem is better integrated in time.

However, when $t_{\mathrm{rev}} = 10$, it was observed that the PS solver better recovers the initial solution than FD4 and that the entrophy was increasing at the end of the backward simulation when using FD4 or $\mathrm{PS}_{\mathrm{w/oT}}$. The spurious increase of the enstrophy was seen to happen when t_{rev} is increased and it corresponds to the enhanced increase of the time-reversibility error seen in Fig. 12. This behavior is probably due to the non-linear interactions of the time-stepping errors. When they become large, the energy transfer between the different scales is altered. The reversed energy cascade that occurs during the backward simulation can be slowed down or even overwhelmed by a spurious forward cascade that makes the enstrophy increase again. It should be noted that the time-reversibility is then less correlated with energy conservation because the variation of the global energy is still due to time-stepping errors while the time-reversibility error is mainly due to a bad distribution of this energy.

These conclusions can be illustrated using 1D examples, that are easier to deal with than the 3D benchmark. Yet, they provide useful insight into the time-reversibility property.

First, to show that dispersion errors are reversible, we can consider the case of the one-dimensional linear convection equation (14). The relation equivalent to (6) is then simply

$$H^h(c,u) = H^h(-c,-u). \tag{17}$$

The exact semi-discrete solution is a sum of modes traveling at a speed c_{eff} depending on the wave number and given by the dispersion relation of the discretization. The time-reversibility test can be performed on this model equation. The simulation is run up to the time t_{rev}, starting from an arbitrary initial condition. Then the signs of the convection velocity c and of the field u are changed and the simulation is run again for the same time. It is easy to see that the dispersion errors do not affect the time reversibility of the scheme because the magnitude of the effective convection velocity of each mode is not affected

by the time reversal (each mode is convected by the same distance but in opposite directions). Only the amplitude error of the time integration affects the time reversibility. The results of this test, using the initial condition $u = u_0 \exp(-x^2/\sigma^2)$, are shown in Fig. 14. The problem is discretized in space using centered second order finite differences:

$$\frac{du_i}{dt} + c\frac{(u_{i+1} - u_{i-1})}{2h} = 0. \tag{18}$$

The dispersion errors of the scheme are clearly visible at time reversal. However, as they are reversible, the final error is only due to the small amplitude error revealed by the small variation of energy. We also note that, for such linear equation, the energy always increases when using AB2 (before and after time reversal), always decreases when using RK3 and is exactly conserved when using Leapfrog.

A more relevant 1D example is the non-linear inviscid Burgers equation

$$\frac{\partial u}{\partial t} + u\frac{\partial u}{\partial x} = 0. \tag{19}$$

Three second order finite difference discretizations of the convective term $H(u)$ can be used:

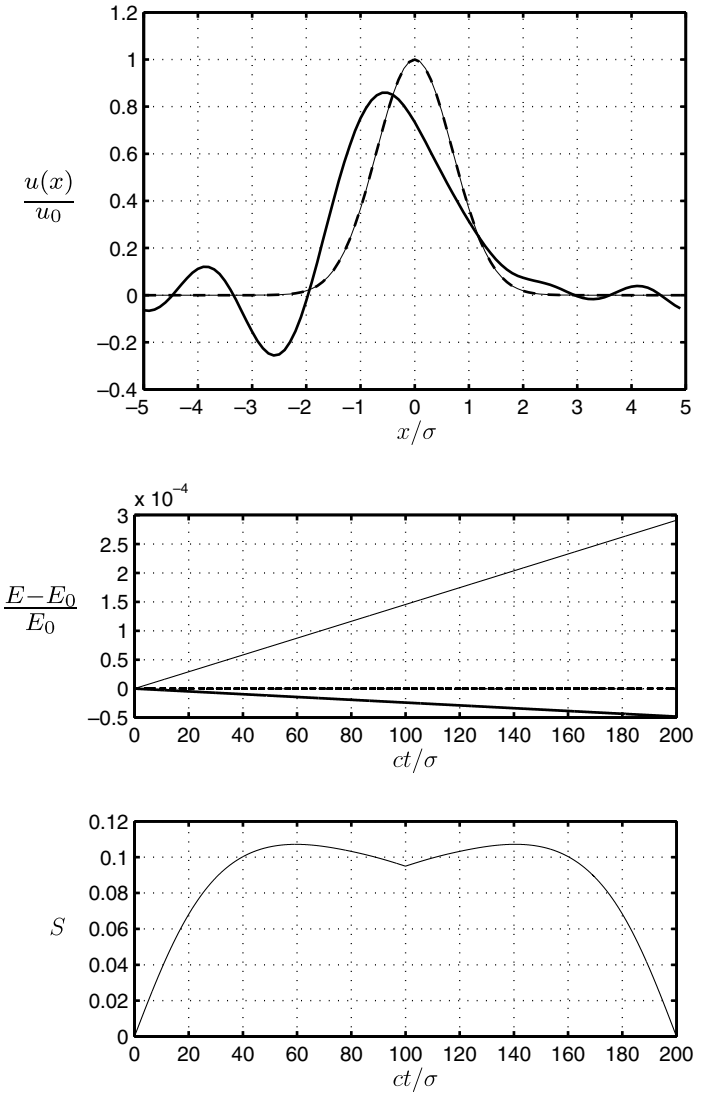

Fig. 14. Time-reversibility of the linear 1D convection equation using second order finite differences. The initial condition is $u/u_0 = \exp(-x^2/\sigma^2)$. The grid size is $h/\sigma = 0.1$ and the time is reversed at $ct/\sigma = 100$. Visualization of the solution obtained using AB2 (above) at times $ct/\sigma = 0$ (thick dash), $ct_{rev}/\sigma = 100$ (thick solid) and $ct/\sigma = 200$ (thin solid). Time history of the energy $(E - E_0)/E_0$ (center) obtained using AB2 (thin), RK3 (thick) and Leapfrog (thick dash). Time history of the skewness $\langle(\partial_x u)^3\rangle/\langle(\partial_x u)^2\rangle^{3/2}$ obtained using AB2 (below).

$$H^h_{\text{adv}} = u_i \frac{(u_{i+1} - u_{i-1})}{2h} \quad \text{Advective form} \tag{20a}$$

$$H^h_{\text{div}} = \frac{1}{2} \frac{(u^2_{i+1} - u^2_{i-1})}{2h} \quad \text{Divergence form} \tag{20b}$$

$$H^h_{skew} = \frac{1}{3} H^h_{\text{adv}} + \frac{2}{3} H^h_{\text{adv}} \quad \text{Skew-symmetric form.} \tag{20c}$$

Only the skew-symmetric form conserves the energy, even though they all satisfy the condition (6). The results of the time-reversibility test using the skew-symmetric form (20c) and the same initial condition as in the linear case are shown in Fig. 15. The exact solution exhibits a discontinuity that cannot be captured by the conservative scheme: it thus accumulates energy in the smallest scales. The numerical solution is non-physical but is still reversible. The error on the energy conservation, and thus the time-integration error, is seen to be larger in the non-linear case than in the linear case. The error increases significantly when the energy starts to pile up in the high wave numbers. Moreover, when using AB2, the energy decreases monotonically after the time reversal, contrary to the linear case. This is similar to the results obtained for the 3D Euler equations (see Fig. 2). This partial reversibility of the amplitude errors thus appears to be a common feature of multi-step schemes applied to non-linear convection equations (it is not the case for the linear convection equation, see Fig. 14). Indeed, it is seen that the leapfrog scheme also exhibits an unstable but reversible behavior (see Fig. 15). Moreover, since it is a time centered scheme, it is perfectly reversible, while AB2 is not. This non-linear

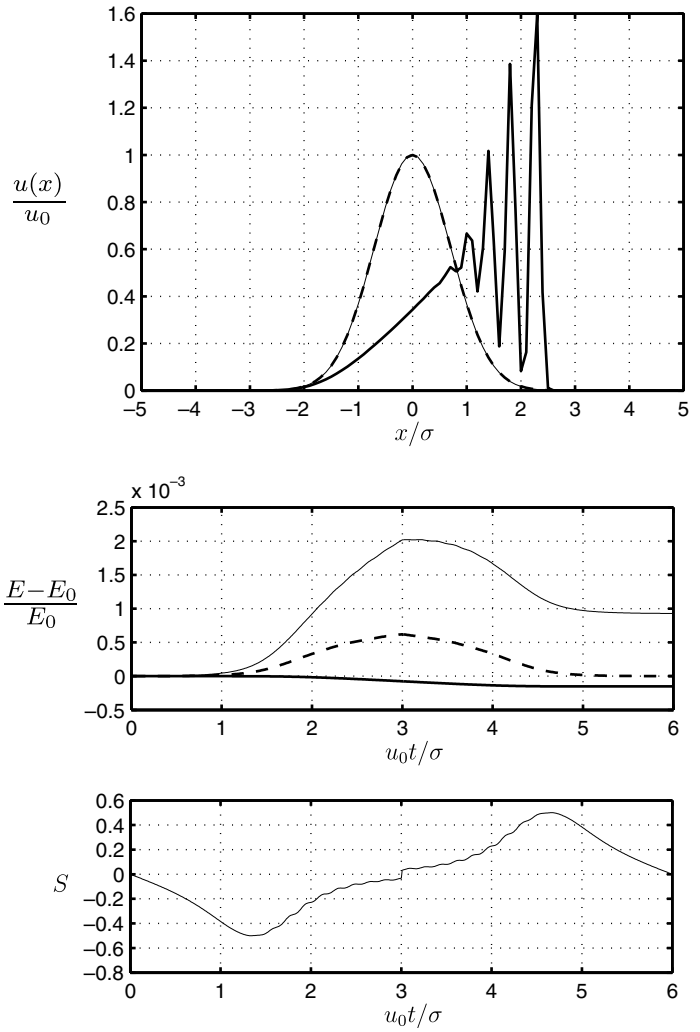

Fig. 15. Time-reversibility of the inviscid Burgers equation using second order finite differences. The initial condition is $u/u_0 = \exp(-x^2/\sigma^2)$. The grid size is $h/\sigma = 0.1$ and the time is reversed at $u_0 t/\sigma = 3$. Visualization of the solution obtained using AB2 (above) at times $u_0 t/\sigma = 0$ (thick dash), $u_0 t_{\text{rev}}/\sigma = 3$ (thick solid), $u_0 t/\sigma = 6$ (thin solid). Time history of the energy $(E - E_0)/E_0$ (center) obtained using AB2 (thin), RK3 (thick) and Leapfrog (thick dash). Time history of the skewness $\langle(\partial_x u)^3\rangle/\langle(\partial_x u)^2\rangle^{3/2}$ obtained using AB2 (below).

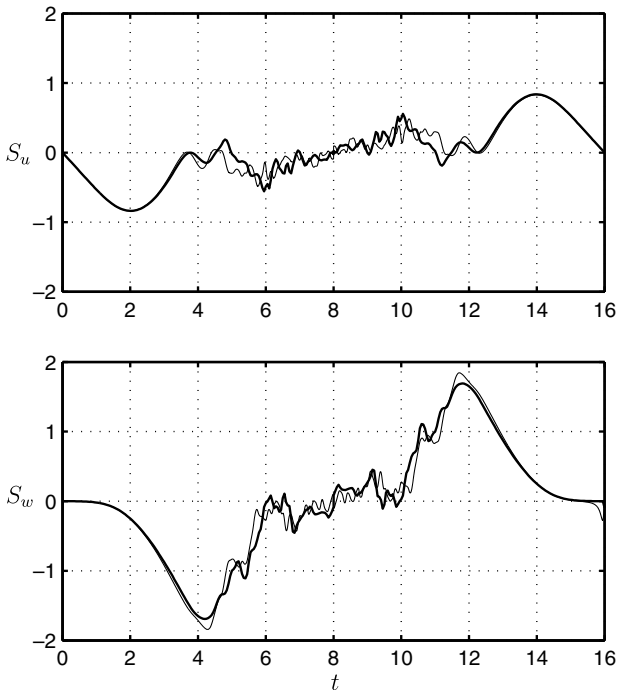

Fig. 16. Time history of the skewness $S_u = \langle(\partial_x u)^3\rangle / \langle(\partial_x u)^2\rangle^{3/2} = S_v$ (above) and of $S_w = \langle(\partial_z w)^3\rangle / \langle(\partial_z w)^2\rangle^{3/2}$ (below) obtained using FD2 (thick) and FD4 (thin), both using AB2.

effect can likely be related to the change in sign of the skewness after the time reversal in both 1D (Fig. 15) and 3D (Fig. 16) cases. Finally, it is seen that multi-substep schemes such as RK3 are not time-reversible for both linear and non-linear problems: they always dissipate energy.

The comparison of the time-history of the energy when using the various discretizations of the convective term is shown in Fig. 17. The three forms are time-reversible and succeed in recovering the initial condition. However, one must be aware that the results obtained in this 1D case with non-conservative schemes cannot be reproduced in 3D because of numerical instabilities.

Finally, and in order to illustrate the reversibility of the aliasing errors, the inviscid Burgers equation can also be solved using the pseudo-spectral method. The spectral discretization read

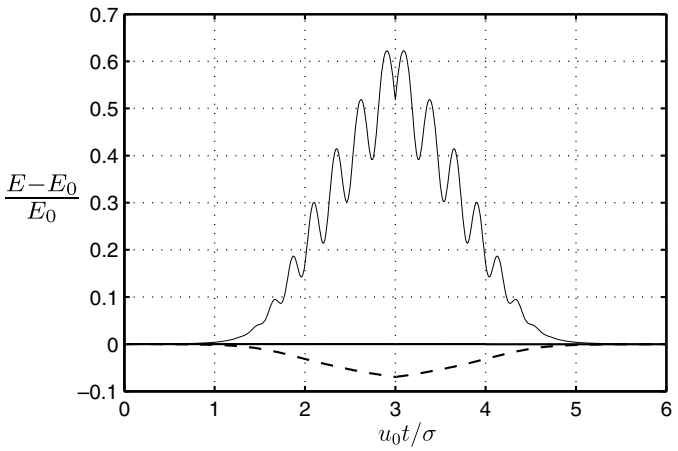

Fig. 17. Time-reversibility of the inviscid Burgers equation using second order finite differences (same setup as Fig. 15). Time history of the energy $(E - E_0)/E_0$ (center) obtained using RK3 and various discretizations of the convective term: Skew-symmetric (thick solid), advective (thin solid) and divergence (dash).

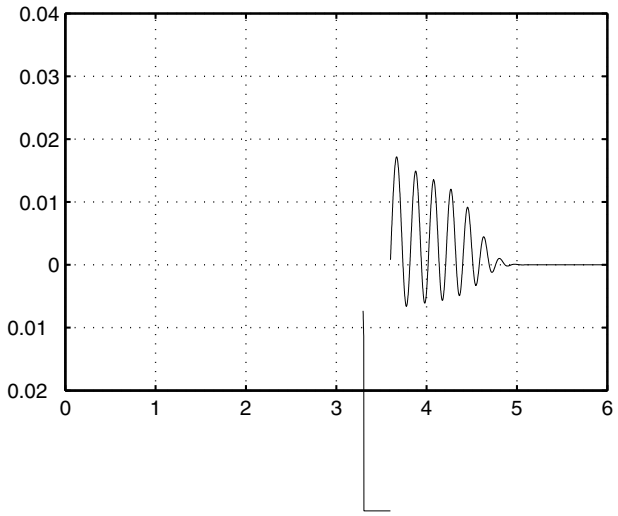

$$\frac{\mathrm{d}\hat{u}_k}{\mathrm{d}t} + \frac{1}{2}\mathrm{i}k \sum_{n+m=k} \hat{u}_n \hat{u}_m + \frac{1}{2}\mathrm{i}k \sum_{n+m=k\pm N} \hat{u}_n \hat{u}_m = 0, \tag{21}$$

where the third term is the aliasing error. This term also verifies (6) and the semi-discrete equation is still reversible. The comparisons of the time-history of the computations with and without dealiasing procedure is presented in Fig. 18. Obviously, the dealiased computation conserves energy and is able to recover the initial condition. But the aliased one does also very well since the aliasing errors are time-reversible.

6. Conclusions

The time-reversibility of various Navier–Stokes solvers running without molecular viscosity, thus in Euler mode, has been investigated. The test consists in running the simulation from the Taylor–Green vortex until the flow has become fully "turbulent". By that time, and as there is no explicit dissipation, much energy has been accumulated in the smallest resolved scales, leading to energy equipartition at the highest wave numbers: $E(k) \propto k^2$. The time is then reversed (or equivalently the sign of the velocity is changed) and the simulation is run again for the same number of time-steps as before. An ideal solver should recover the initial condition. The solvers tested here succeed very well in recovering the initial condition, provided that the time-step is small and that the time reversal does not occur too late.

Theoretically, it was shown that most space discretizations would be reversible if the time integration was exact. This means that the errors associated with the space discretization, such as the dispersion errors or aliasing errors, are reversible. The energy conservation appears to be a requirement for the space discretization in order to be able to recover the initial condition in 3-D flows. The accuracy of the time-stepping scheme is then found to be crucial to obtain good time-reversibility properties. However, the interaction between the time-stepping scheme and the space discretization can also be important and is at the origin of the differences between the solvers using the same time-stepping scheme. This interaction determines the energy conservation properties of the solver and it was observed that the best time-reversible solvers also have the best energy conservation capabilities. In the present investigation, it turned out that the best solver for this test used second order finite differences.

As the requirement to pass the time-reversibility test are (1) to be energy conserving and (2) to be highly accurate in time, it constitutes a severe test that Navier–Stokes solvers should challenge. The present benchmark is therefore proposed to the community. The required skills are also fundamental for solvers designed to perform Large-Eddy Simulations using explicit subgrid-scale modeling (thus without dissipation expected when the model is turned off). Finally, they are also fundamental for solvers used to investigate the possibility of finite time singularity in the Euler equations.

Acknowledgments

Matthieu Duponcheel is funded by the *Fonds de la Recherche Scientifique FNRS* and has a position as FNRS Research Fellow. The FD4 solver was initially developed at UCL by Laurent Georges (presently at CENAERO). The PS solver was provided by Pr. Hervé Jeanmart (UCL/TERM). The computing resources used at UCL were provided by the CISM (*Institut de Calcul Intensif et de Stockage de Masse*) where the cluster *Lemaître* was used. This cluster was funded by FNRS (Fonds de la Recherche Fondamentale Collective – FRFC) and UCL (Fonds spéciaux de recherche) with the project FRFC 2.4502.05 "Simulation numérique:

Application en physique de l'état solide, océanographie et dynamique des fluides". The simulations using the second order scheme were supported by a MPI 60% grant.

References

[1] D. Carati, G. Winckelmans, H. Jeanmart, On the modelling of the subgrid-scale and filtered-scale stress tensors in large-eddy simulation, J. Fluid. Mech. 441 (2001) 119–138.
[2] P. Orlandi, G.F. Carnevale, Nonlinear amplification of vorticity in inviscid interaction of lamb dipoles, Phys. Fluids 19 (5) (2007) 057106.
[3] M. Lee, B. Oh, Y. Kim, Canonical fractional-step methods and consistent boundary conditions for the incompressible Navier–Stokes equations, J. Comput. Phys. 168 (2001) 73–100.
[4] Y. Morinishi, T.S. Lund, O.V. Vasilyev, P. Moin, Fully conservative higher order finite difference schemes for incompressible flow, J. Comput. Phys. 143 (1) (1998) 90–124.
[5] P. Orlandi, Fluid Flow Phenomena – A Numerical Toolkit, Kluwer Academic Publishers, Dordrecht, 2000.
[6] O. Vasilyev, High order finite difference schemes on non-uniform meshes with good conservation properties, J. Comput. Phys. 157 (2) (2000) 746–761.
[7] J. Williamson, Low-storage Runge–Kutta schemes, J. Comput. Phys. 35 (1980) 48–56.
[8] C. Canuto, M. Hussaini, A. Quarteroni, T. Zang, Spectral Methods in Fluid Dynamics, Springer-Verlag, 1988.
[9] M.E. Brachet, D.I. Meiron, S.A. Orszag, B.G. Nickel, R.H. Morf, U. Frisch, Small-scale structure of the Taylor–Green vortex, J. Fluid Mech. 130 (1983) 411–452.
[10] J. Jeong, F. Hussain, On the identification of a vortex, J. Fluid Mech. 285 (1995) 69–94.
[11] C. Pierce, P. Moin, Progress-variable approach for large-eddy simulation of non-premixed turbulent combustion, J. Fluid Mech. 504 (2004) 73–97.